3D-Spiral Small Antenna Design and Realization for Biomedical Telemetry in the MICS band

Javier ABADIA[1,2]*, Francesco MERLI*[1]*, Jean-François ZURCHER*[1]*,*
Juan R. MOSIG[1]*, Anja K. SKRIVERVIK*[1]

[1]Lab. d'Electromagnét. et d'Acoust., Ecole Polytechnique Féd. de Lausanne, Station 11, CH-1015 Lausanne, Switzerland
[2]Syderal SA, Neuenburgstrasse 7 3238-Gals, Switzerland. Formerly with El. Engg. and Comm. Dpt., Univ. Zaragoza, Spain

javier.abadia@syderal.ch, francesco.merli@epfl.ch

Abstract. *This work presents the design and realization procedure of small implantable antenna for biotelemetry applications. The radiator occupies a volume smaller than 3 cm*^{3} *(without its biocompatible insulation), is well matched within the Medical Implanted Communications System band and shows an adequate gain (-28.5 dB) while introduced in the appropriate equivalent body medium. The latter is a homogeneous phantom with muscle dielectric properties. A prototype has been manufactured and measurements agree with theoretical predictions. Particular attention is paid to the building requirements such as the presence of glue. Specific Absorption Rate (SAR) distribution has been computed evaluating the maximum power deliverable to the antenna in order to respect the regulated SAR limitation.*

Keywords

Electrically Small Antenna (ESA), implantable antenna, Medical Implant Communications Services (MICS), Medical Device Radiocommunication Service (MedRadio), biocompatible antenna.

1. Introduction

During the last decades, biomedical engineering has experienced a remarkable growth. Among others, the design of bio-implantable devices, that help people to improve their health care and quality of life, has attracted a lot of interest [1], [2], [3], [4]. When considering biotelemetry systems, the study of the communication devices used for establishing a wireless link between the implanted device and the external base station becomes essential. In this sense, the implanted system must fulfill two main requirements: miniaturization and good radiation performances.

Historically, low-frequency inductive links have been the most prevalent way of transmitting very short range communication links. Nowadays the Medical Implanted Communications Services band (MICS, 402-405 MHz) [5], [6] or the Medical Device Radiocommunication Service band (MedRadio, 401-406 MHz) [7], [8] are specifically allocated for this application. This allows for longer range communications but, as a drawback, makes the traditional $\lambda/2$ or $\lambda/4$ antennas useless. In fact, their dimensions would not be small enough to be implanted in the human body. Hence the radiator, as well as the front element of the system, must be designed with particular care [9]- [17].

This work presents the design and realization of an implantable antenna extending the preliminary results of [18]. The radiator operates in the MICS band, occupies a volume smaller than 3 cm^3 (without its biocompatible insulation) and shows a gain of -28.5 dB including body losses. This low gain value implies a poor radiation efficiency indeed, but it is still suitable for a personal area network communication using some already available transducers (e.g. [19]).

This manuscript is organized as follows: Section 2 presents the strategy and the optimization procedure followed to reach the prefixed performances while Section 3 introduces the final design and illustrates the effects of peculiar aspects such as the glue presence or the use of different body phantoms. Moreover the Specific Absorption Rate (SAR) distribution is reported here to compute the maximum power deliverable to the antenna in order to respect the regulated SAR limitation [20]. Section 4 shows the building process and, finally, Section 5 describes the experimental results of the realized prototype.

2. Antenna Design Strategy

Designing an antenna from scratch, taking into account the body and its losses, would be a tedious process as the simulation time involved would be very large. Thus, in the first step, the antenna is designed in free space and we aim for a gain value higher than -20 dB since body absorption losses are not present. As a starting point for the design procedure, the volume occupation is initially limited to 10 cm^3, which corresponds to a cube with a side measuring 2.15 cm.

As previously mentioned, a traditional quarter wave or half wave antenna would have sizes either of 18 or 37 cm in the selected frequency band, which is clearly unrealistic for the implantation into the human body. As a consequence, miniaturization techniques like those described in [21] must be used in order to reduce the antenna's dimensions. Among these techniques, *dielectric loading*, and the use of *grounding pins* (PIFA antennas), have been shown to be very effective ways of reducing the dimensions of the antenna, while maintaining adequate electromagnetic performance [21], [22], [23].

A possible way to ensure the required gain is to depart from classic PIFA antennas and to consider a thicker structure. As a consequence, the lateral substrate faces may provide extra surfaces for the design of a three-dimensional radiator. In addition, keeping in mind the good performance of *normal-mode helical antennas* [23], we consider a complex structure combining all the previous characteristics. Fig. 1 shows the first design steps, starting from a planar model to a three dimensional radiator and finally showing the structure with a double dielectric substrate and a 3D-spiral metallization. The lower substrate provides the standard substrate above the ground plane while the spiral metallization is wound around the upper substrate.

2.1 Free Space Optimization

To achieve optimal performances, an iterative miniaturization method has been undertaken. It consists of performing a series of optimizations that leads to the maximum volume reduction while still obtaining the desired electromagnetic behavior of the antenna. This procedure is applied following the scheme reported in Fig. 2 with the use of Ansoft HFSS [24]. It is worth noting at this point,

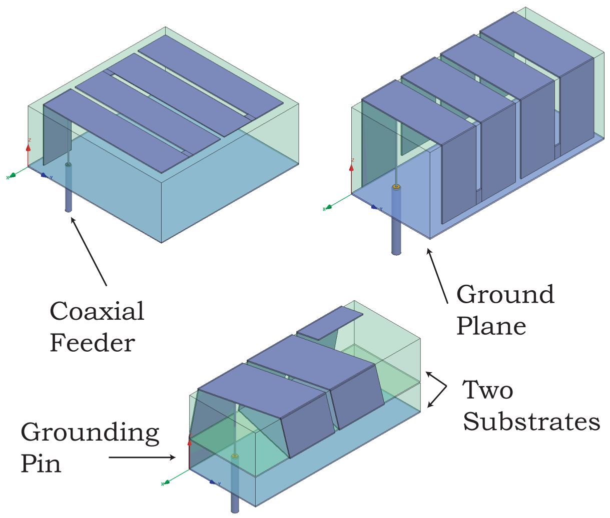

Fig. 1. First design steps leading to a 3D-spiral structure.

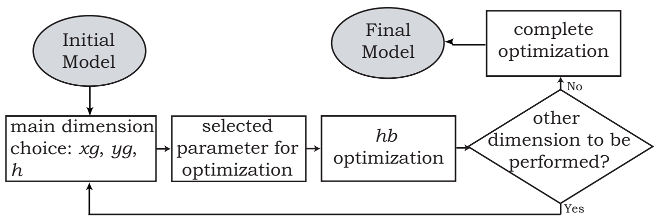

Fig. 2. Scheme of the optimization procedure.

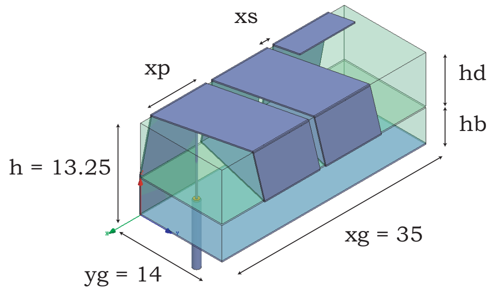

Fig. 3. Design and main dimensions in [mm] of the starting structure to be optimized.

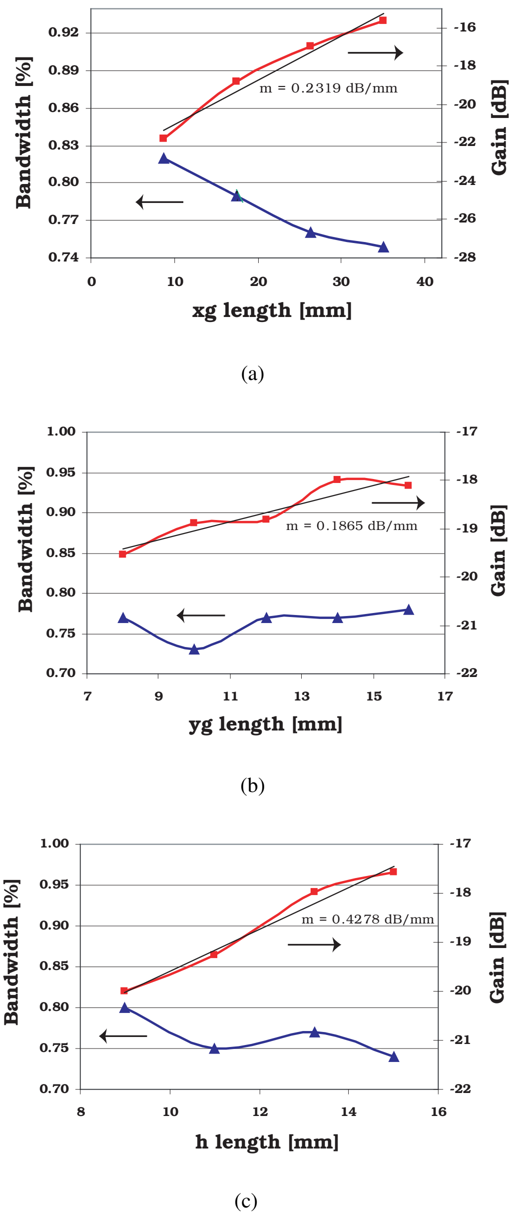

Fig. 4. Gain and bandwidth trend versus different dimensions on the three main axes.

that the simulations are performed considering the antenna alone in a free space environment.

The starting design consists of a short-circuited folded rectangular patch forming a 3D-spiral over the ground plane as depicted in Fig. 3.

Each of the three main dimensions bounding the antenna volume (xg, yg, h in Fig. 3) has been reduced while keeping constant the resonant frequency of 400 MHz (with a tolerance of ±2 %). This is accomplished by changing the thickness of the lower substrate, hb, and allows for a fair comparison of the different results. Fig. 4 shows the performance in terms of gain and bandwidth, associated to the variation of xg, yg and h. As expected, a decrease in any dimension always involves a gain reduction, due to the smaller volume occupied by the antenna.

After reducing the antenna dimensions on all its 3 axes, a complete optimization is performed by analyzing several spiral configurations, as depicted in Fig. 5. Parameters such as the width of the metallic strip, xp, and the gap between the spiral loops, xs (Fig. 3), as well as the number of metallic turns around the superior substrate, are consequently modified while still maintaining the resonance frequency constant at around 400 MHz.

The last step of the procedure includes the choice of the dielectric material. Since the design process calls for the use of two separate substrates, several possibilities combining Teflon and a ceramic material (HIK500 [25], ε_r = 11) have been analyzed. As expected, simulation results show that the use of the higher relative permittivity material leads to a smaller yet still efficient antenna. Hence, the ceramic substrate was chosen for this prototype. Once the iterative procedure is finished, the antenna dimensions are 14×14×15 mm, (Fig. 6). The radiator shows a maximum gain of -17.57 dB, 0.75 % of relative bandwidth centered at 402 MHz as reported in Fig. 7. As the antenna is electrically very small, the radiation pattern, depicted in Fig. 7, is omnidirectional.

In summary, Tab. 1 shows the initial and the final 3D-spiral antennas' characteristics. The total volume was successfully reduced to 55 %, while only losing 1.4 dB on gain and maintaining the bandwidth during the optimization process.

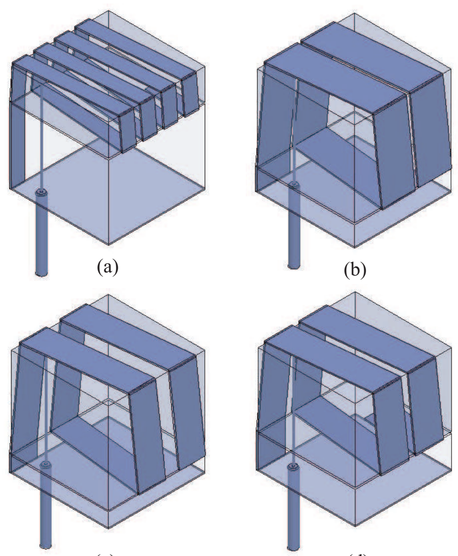

Fig. 5. Different spiral designs that have been analyzed, among all the explored possibilities, to improved the obtained performance while keeping the volume constant.

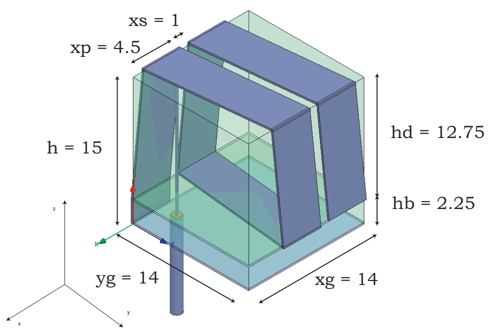

Fig. 6. Geometry and dimensions [mm] of the optimized design.

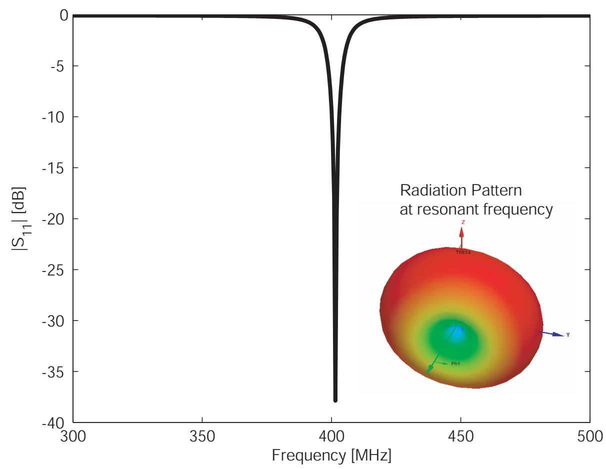

Fig. 7. Matching Performance and 3D radiation pattern of the final structure considering a free space environment.

Characteristics	Initial (free space)	Final (free space)
Dimensions	35×14×13.25 mm	14×14×15 mm
Volume	6.49 cm^3	2.94 cm^3
Bandwidth	0.75 %	0.75 %
Gain	-16.18 dB	-17.57 dB
Resonant frequency	399 MHz	402 MHz
VSWR	1.057	1.117

Tab. 1. Antenna's characteristics before and after the optimization process performed in free space.

3. Complete Final Design

After the optimization of the radiator in free space, it is necessary to introduce biocompatible insulation and the human body model. In order to simplify the analysis, the antenna is placed at the center of an equivalent body medium following the recommendation of [6]. This 'body phantom' is a homogeneous cylinder with dielectric properties to those of a real muscle tissue: $\varepsilon_r = 57.1$, $\tan\delta = 0.622$ and $\sigma = 0.796$ S/m [26]. Due to an eventual subcutaneous placement for practical applications, the cylinder has a radius of 4 cm, which corresponds to a body thickness of approximately 30 mm as shown in Fig. 8, with a height of 10 cm.

PEEK ($\varepsilon_r = 3.2$, $\tan\delta = 0.01$, produced by [27]) is chosen as the biocompatible layer. The insulation is needed in order to avoid any direct contact of the human body with the antenna. This prevents the rejection of the implant and undesired short-circuits of the radiator due the conductive body tissues.

Due to the presence of muscle and PEEK, the antenna's electromagnetic properties change, but the knowledge acquired during the optimization procedure in free space facilitates the necessary corrections. Thus, only the relocation of the feed and a variation of the substrates' thicknesses, *hb* and *hd*, are required, while considering the same volume.

The effects of the variation of the biocompatible material thickness (from 1 to 4 mm) have been analyzed and its optimum value is found to be at 1.5 mm, see Fig. 9. For this case, the gain attains a maximum value of -28.50 dB and the resonant frequency is located at 405 MHz, with a -10 dB bandwidth of 225.5 MHz (55.7 %), as shown in Fig. 9. The obtained matched band is much larger than the one for the free space case. This feature is clearly related to the introduction of the equivalent muscle medium. In fact, the lossy material absorbs most of the incident power reducing considerably reflected power. Introducing the insulation layer and the muscle tissue makes the antenna electrically larger, compared to the free space case analyzed in Section 2.1, and this implies a small directivity improvement as depicted in Fig. 9. Polarization is prevalently elliptical but this is not of great interest for such a small antenna for indoor applications [23].

Comparing different implantable antennas is not straightforward since different body models, in terms of dielectric properties, shape and dimensions, can be considered. Despite this fact, the most relevant performances of our antenna are compared with alternative designs [9], [12], [13], [15] in Tab 2.

It can be noted how the proposed model shows an adequate gain (higher than -30 dB) considering a remarkably thicker lossy medium, but this is at the cost of a larger occupation volume.

3.1 Glue effect

During the building process, an additional glue layer ($\varepsilon_r = 3$, $\tan\delta = 0.001$) will be used to affix all the components. Since this extra layer is obviously in contact with the metallic and dielectric materials (both ceramics and insulation) it is important to take its influence into account.

Fig. 10 shows the reflection coefficients versus frequency, $|S_{11}(f)|$, obtained for different glue layer thicknesses. As expected, the thicker the glue layer is, the more the resonant frequency shifts, and the higher the mismatch becomes. Thus, the metallization of the antenna has to be slightly adjusted to take this shift into account.

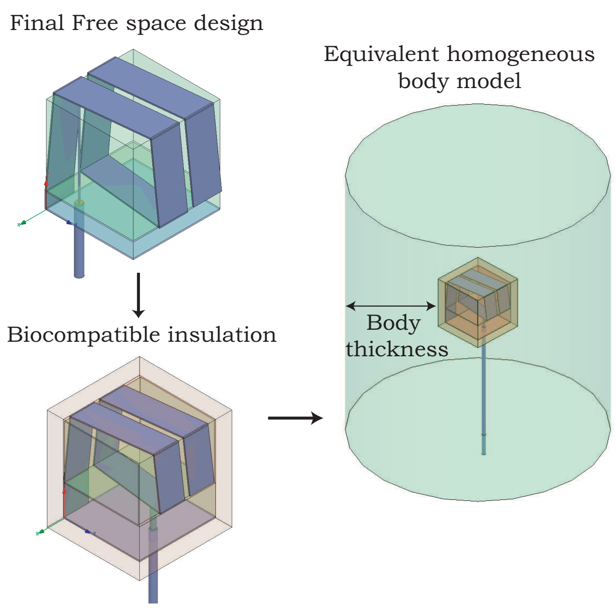

Fig. 8. Scheme of the introduction of the insulation layer and the equivalent body model.

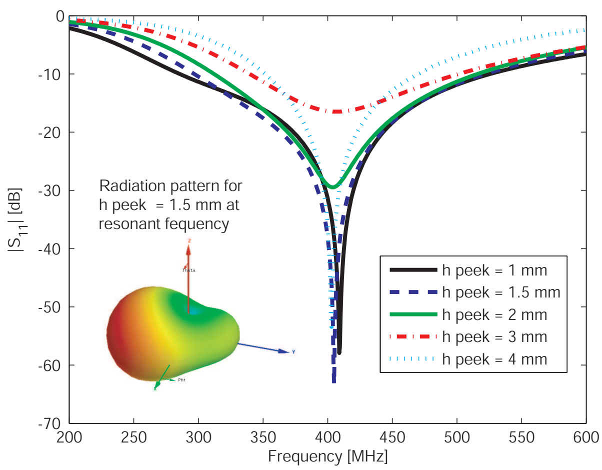

Fig. 9. Simulated $|S_{11}|$ variation due to different insulation thicknesses and 3D radiation pattern of the final design.

Solution	Antenna's volume [mm^3] with insulation	Body model	Min. Body thickness [mm]	Max Gain [dB]
[9]	$17\times27\times6 = 2754.0$	2/3 muscle, $\varepsilon_r = 42.80$, $\sigma = 0.64$	7	-35
[13]	$22.5\times22.5\times2.5 = 1265.6$	skin mimic gel, $\varepsilon_r = 46.74$, $\sigma = 0.68$	3	-25
[12]	$7.5^2\times\pi\times1.9 = 335.7$	skin, $\varepsilon_r = 46.70$, $\sigma = 0.69$	4	-26
[15]	$11.5^2\times\pi\times24.72 = 10271.0$ (including electronics and power supply)	muscle, $\varepsilon_r = 57.10$, $\sigma = 0.79$	$\simeq 20$	-29
proposed	$17\times17\times18 = 5202.0$	muscle, $\varepsilon_r = 57.10$, $\sigma = 0.79$	31	-28.5

Tab. 2. Antennas' characteristics comparison.

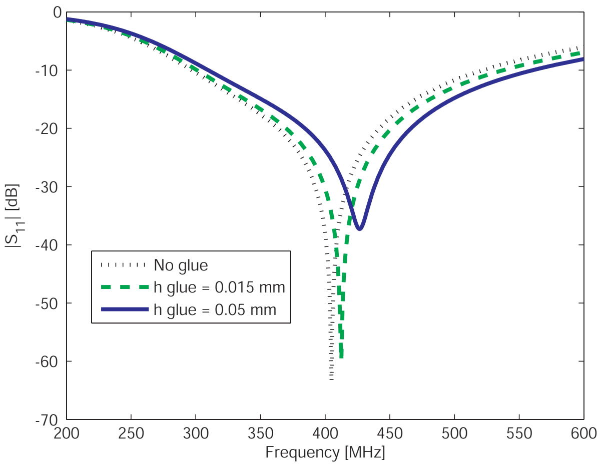

Fig. 10. Simulated $|S_{11}(f)|$ variation due to different glue layer thicknesses.

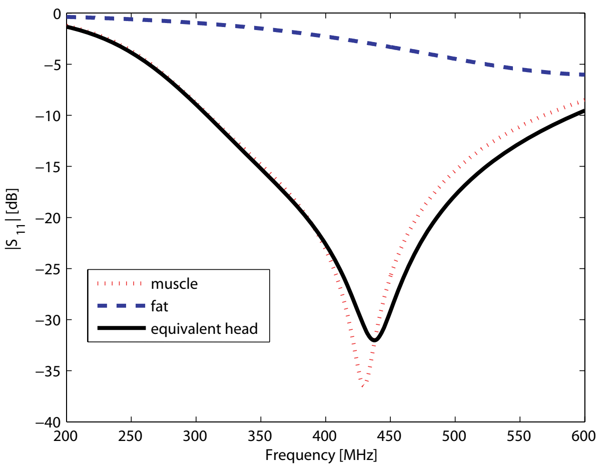

Fig. 11. Simulated $|S_{11}(f)|$ variation due to different body phantoms: muscle and fat from [26], equivalent head from [20] .

3.2 Body Phantoms

Since our body phantom is a rather rough approximation of the real human model, it is important to evaluate the robustness of the electromagnetic performances in different environmental conditions. Hence, simulated reflection coefficients against the frequency, $|S_{11}(f)|$, are shown in Fig. 11 considering the presence of 3 distinct homogeneous body phantoms, namely:

- homogeneous muscle, $\varepsilon_r = 57.10$, $\tan\delta = 0.622$,
- homogeneous head model from [20], $\varepsilon_r = 43.50$, $\tan\delta = 0.790$,
- homogeneous fat, $\varepsilon_r = 5.57$, $\tan\delta = 0.329$.

The obtained results illustrate that the proposed antenna has a stable behavior versus the selection of homogeneous phantoms. In fact, the use of muscle or the equivalent head model does not remarkably affect its matching characteristic. A change of around 25% in the dielectric constant only modifies the resonant frequency of 2%. On the other hand this stable behavior has its limits and it no longer applies to the fat case where the large dielectric variation (around of 1 order of magnitude smaller with respect to the other models) sends the antenna completely out of the desired frequency band.

3.3 Specific Absorption Rate

Specific Absorption Rate (SAR) in the homogeneous muscle equivalent phantom is computed using a commercial EM simulator [24]. This gives a fair idea of the power absorbed by the body model. To obtain more realistic results and evaluate the induced thermal effects, a much more detailed and complex body phantom should be used, for instance taking into account the blood flow and thermal regulation, as pointed out in [28]. Nevertheless, the simple approximation made here is a useful first indication.

At the current level of our on-going research project, no specific active electronics have been yet developed for a future integration. Therefore we must test our prototype with an external coaxial cable feed. This strongly affects the SAR distribution and is expected to have an influence on the performance of the antenna itself.

Even if the final implanted system may be different, it is important to simulate and measure the same structure in order to verify our design strategy. In fact, since the radiator is electrically small, the transition from the coaxial cable to the radiator generates currents flowing along the outer conductor [29]. These are dissipated in the lossy body medium and will modify both the simulations and the measurements.

As mentioned above, the maximum SAR values are distributed in close proximity of the feeding cable. Providing the antenna with a 1 W input signal, the 1-g averaged SAR distribution over the *yz*-plane (at the excitation position) is depicted in Fig. 12. In order to satisfy the IEEE recommendation (2 W/kg, see [30]) the power delivered to the antenna should be decreased to 7.4 mW.

4. Construction Process

In order to validate the design, a prototype has been built, as shown in Fig. 13. Even if the structure is rather complex, a simple construction procedure was required since the metallization is folded around the two dielectric pieces. The antenna is composed of a 200 μm thick copper-beryllium metallization, two HIK500 ceramic substrates (ε_r = 11, $\tan\delta$ = 0.01) and is covered by PEEK. All the used materials have been characterized by measurements.

The equivalent body model was realized with a liquid solution following the recipe reported in [11]. In order to ensure that its electromagnetic characteristics agreed with the theoretical ones, its complex permittivity was measured using the HP Dielectric Probe Kit 85070E [31] and found in agreement with the predictions, as reported in Tab. 3.

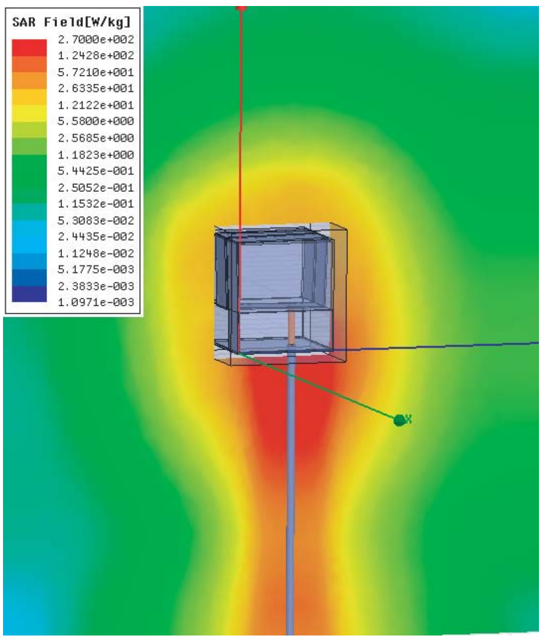

Fig. 12. Simulated surface 1-g averaged SAR distribution over the *yz*-plane (at the excitation position).

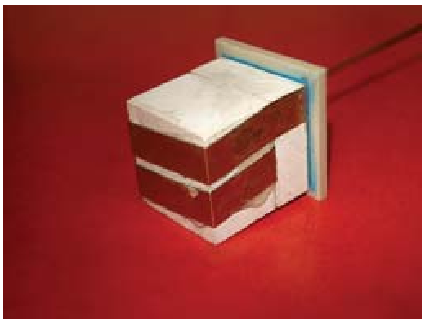

(a)

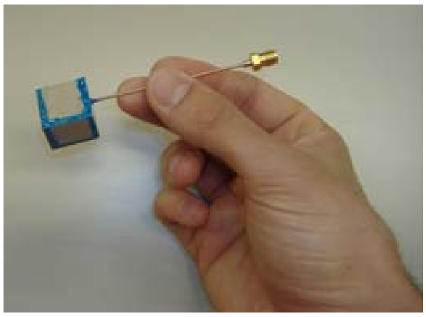

(b)

Fig. 13. Realization of the prototype: (a) intermediate and (b) final structure.

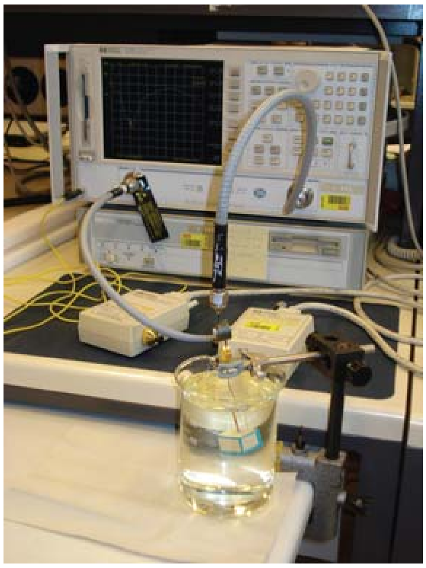

Fig. 14. Measurements setup to check the realized antenna performance in the equivalent body medium.

Target values [26]	**Measured values**
ε_r = 57.10, $\tan\delta$ = 0.622	ε_r = 57.21, $\tan\delta$ = 0.626

Tab. 3. Equivalent body medium dielectric properties.

5. Measurements

The measurement of an implantable radiator is rather complex, since it combines the inherent problems of ESA testing [29] and the presence of an equivalent body medium. In order to accomplish stable and repetitive conditions, a particular setup has been built, as shown in Fig. 14. Experimental results, using a choke to reduce the current flow on the cable connecting to the Network Analyzer, confirmed the simulated results, as shown in Fig. 15.

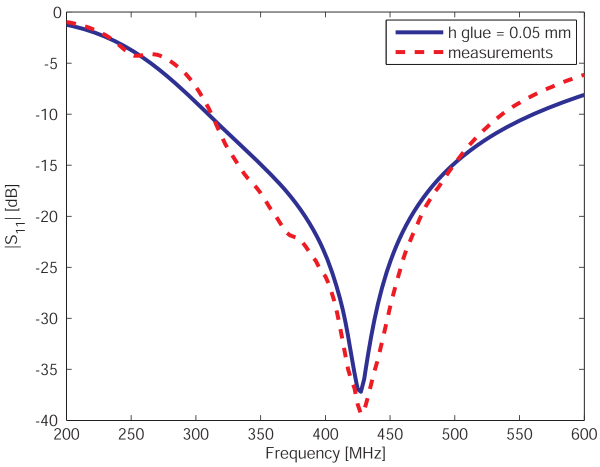

Fig. 15. comparison of the simulated and measured $|S_{11}(f)|$ for the realized prototype.

6. Conclusion

This work describes the design and realization procedure of an implantable antenna. The design strategy used was successful in reducing the needed simulation time. Moreover, it allowed us to understand and to evaluate the influences of each of the elements constituting the radiator. This is very valuable since ulterior modifications (for instance including the glue presence) are then straightforward.

The implantable antenna was tested while inserted into a cylindrical homogeneous body phantom with muscle like properties. The presented prototype shows a wide matching band (225 MHz centered at 427 MHz) that is obviously due to the muscle medium presence. In fact, the lossy material absorbs most of the incident power reducing considerably reflected power. The radiator shows an adequate gain (-28.50 dB) while occupying a volume smaller than 3 cm^3 (without its biocompatible insulation). Since the design is still dependent on the feeding transmission line, a final optimization procedure is envisaged for a future integration of the required transceiver and power supply.

Experimental results are in agreement with simulated ones, revealing the importance of a good characterization of all the materials used in both the antenna's design and realization. Both the insulation layer and the presence of glue noticeably affect the resonant frequency, and must be taken into account to reach the desired design specifications.

The robustness of the design in different environmental conditions (i.e. different body phantoms) has been verified and shows good performance.

Finally, the maximum power deliverable to the antenna in order to fulfill the existing regulations [20] has been computed by evaluating the SAR distribution.

Acknowledgements

We would like to thank *Angst+Pfister* [32] for providing the samples of PEEK used during the realization of the presented prototype.

References

[1] GREATBATCH, W., HOLMES, C. F. History of implantable devices, *IEEE Engineering in Medicine and Biology*, 1991, vol. 10, no. 3, p. 38–49.

[2] ROSEN, H. D., ROSEN, A., VANDER VORST, A. Biological effects and medical applications. In *Proc. 27th European Microwave Conference, Vol. 2*. 1997, p. 984–991.

[3] ROSEN, A., STUCHLY, M. A., VANDER VORST, A. Applications of RF/microwaves in medicine. *IEEE Transactions on Microwave Theory and Techniques*, 2002, vol. 50, no. 3, p. 963–974.

[4] BANSAL, R. Coming soon to a hospital near you! [biomedical applications of RF/microwaves]. *IEEE Microwave Magazine*, 2002, vol. 3, no. 3, p. 34–36.

[5] Federal Communication Commission. *Medical Implant Communications Service (MICS), (FCC) Std. CFR*, Part 95, 1999.

[6] European Telecommunications Standards Institute. *Electromagnetic compatibility and Radio spectrum Matters (ERM); Short Range Devices (SRD); Ultra Low Power Active Medical Implants (ULP-AMI) and Peripherals (ULP-AMI-P) operating in the frequency range 402 MHz to 405 MHz; Part 1 and Part 2, ETSI Std. EN 301 839-1/2 V1.3.1*. 2007.

[7] Federal Communication Commision. *Medical Device Radiocommunication Service (MedRadio)*, FCC Std., 2009. [Online]. Available at: http://www.fcc.gov/

[8] European Telecommunications Standards Institute. *Electromagnetic compatibility and Radio spectrum Matters (ERM); Ultra Low Power Active Medical Implants (ULP-AMI) operating in the 401 MHz to 402 MHz and 405 MHz to 406 MHz bands; System Reference Document, ETSI Std. TR 102 343 V1.1.1*. 2004.

[9] SOONTORNPIPIT, P., FURSE, C., CHUNG, Y. C. Design of implantable microstrip antenna for communication with medical implants. *IEEE Transactions on Microwave Theory and Techniques*, 2004, vol. 52, no. 8, p. 1944–1951.

[10] KIM, J., RAHMAT-SAMII Y. Implanted antennas inside a human body: simulations, designs, and characterizations. *IEEE Transactions on Microwave Theory and Techniques*, 2004, vol. 52, no. 8, p. 1934–1943.

[11] HALL, P. S., HAO, Y. *Antennas and Propagation for Body-centric Wireless Communications*. Norwood: Artech House, 2006.

[12] LEE, C. M., YO T. C., LUO, C. H., TU, C. H., JUANG, Y. Z. Compact broadband stacked implantable antenna for biotelemetry with medical devices. *Electronics Letters*, 2007, vol. 43, no. 12, p. 660–662.

[13] KARACOLAK, T., HOOD, A. Z., TOPSAKAL, E. Design of a dual-band implantable antenna and development of skin mimicking gels for continuous glucose monitoring. *IEEE Transactions on Microwave Theory and Techniques*, 2008, vol. 56, no. 4, p. 1001–1008.

[14] KARACOLAK, T., TOPSAKAL, E. Electrical properties of nude rat skin and design of implantable antennas for wireless data telemetry. In *Proc. IEEE MTT-S International Microwave Symposium*. 2008, p. 907–910.

[15] MERLI, F., BOLOMEY, L., MEURVILLE, E., SKRIVERVIK, A. K. Implanted antenna for biomedical applications. In *Proc. IEEE Antennas and Propagation Society International Symposium AP-S 2008*. 2008, p 1–4.

[16] YILMAZ, T., KARACOLAK, T., TOPSAKAL, E. Characterization and testing of a skin mimicking material for implantable antennas operating at ISB band (2.4 GHz-2.48 GHz). *IEEE Antennas and Wireless Propagation Letters*, 2008, vol. 7, p. 418–420.

[17] KARACOLAK, T., COOPER, R., TOPSAKAL, E. Electrical properties of rat skin and design of implantable antennas for medical wireless telemetry. *IEEE Transactions on Antennas and Propagation*, 2009, vol. 57, no. 9, p. 2806–2812.

[18] ABADIA, J., MERLI, F., ZURCHER, J.-F., MOSIG, J. R., SKRIVERVIK, A. K. 3D-spiral small antenna for biomedical transmission operating within the mics band. In *Proc. 3rd European Conference on Antennas and Propagation EuCAP 2009*. Berlin (Germany) 2009, p. 1845–1849.

[19] Zarlink Semiconductors. *Integrated Circuit ZL70101*. [Online]. Available at: http://www.zarlink.com

[20] Federal Communication Commission. *Evaluating Compliance with FCC Guidelines for Human Exposure to Radiofrequency Electromagnetic Fields, FCC Std. Supplement C*, OET Bulletin 65, Edition 97-01, 2001.

[21] SKRIVERVIK, A. K., ZURCHER, J. F., STAUB, O., MOSIG, J. R. PCS antenna design: the challenge of miniaturization. *IEEE Antennas and Propagation Magazine*, 2001, vol. 43, no. 4, p. 12–27.

[22] RAHMAT-SAMII, Y., and KIM, J. *Implanted Antennas in Medical Wireless Communications*. USA: Morgan & Claypool, 2006.

[23] FUJIMOTO, K., HENDERSON, A., HIRASAWA, K., JAMES, J. *Small Antennas*. 1st Ed. Letchworth: Electronic & Electrical Research Studies Press, 1987.

[24] Ansoft Corporation. *High Frequency Structure Simulator (HFSS) v11.1 (2009)*. [Online]. Available at: http://www.ansoft.com/products/hf/hfss/

[25] *Emerson & Cuming*. [Online]. Available at: http://www.emersoncuming.com/

[26] GABRIEL, C. *Compilation of the Dielectric Properties of Body Tissues at RF and Microwave Frequencies*, technical report N.AL/OE-TR-. Texas (USA): Brooks Air Force Base, 1996. [Online]. Available at: http://niremf.ifac.cnr.it/tissprop/htmlclie/htmlclie.htm

[27] *Victrex® PEEK™ polymers*. [Online]. Available at: http://www.victrex.com/en/products/victrex-peek-polymers/victrex-peek-polymers.php

[28] WAINWRIGHT, P. R. The relationship of temperature rise to specific absorption rate and current in the human leg for exposure to electromagnetic radiation in the high frequency band. *Physics in Medicine & Biology*, 2003, vol. 48, no. 19, p. 3143–3155.

[29] SKRIVERVIK, A. K., ZURCHER, J. F. Recent advances in PCS antenna design and measurement. *AUTOMATIKA-Journal for Control, Measurement, Electronics, Computing and Communications*, 2002, vol. 43, no. 1-2, p. 55–61.

[30] IEEE. *Standard for Safety Levels with Respect to Human Exposure to Radio Frequency Electromagnetic Fields, 3 kHz to 300 GHz*. IEEE Std. Std C95.™-, 2005.

[31] Agilent Technologies. *Agilent 85070e Dielectric Probe Kit 200 MHz to 50 GHz Technical Overview, Tech. Rep.* [Online]. Available at: http://cp.literature.agilent.com/litweb/pdf/5989-0222EN.pdf

[32] *Angst+Pfister*. [Online]. Available at: http://www.angst-pfister.com/en/DesktopDefault.aspx/tabid-1/

About Authors...

Javier ABADIA was born in Zaragoza, Spain, in 1982. He received an Engineering degree in Telecommunications from the University of Zaragoza in 2008. He was awarded the Best Master's Project Award by The Official College of Telecommunications Engineers in Aragon, for his work developed at the Ecole Polytechnique Fédérale de Lausanne, Switzerland. He is currently working at Syderal SA on the design of communication and electronic systems mounted on European Space Agency's spacecrafts.

Francesco MERLI was born in Faenza, Italy, in 1981. He received the laurea degree (cum laude) in Telecommunication Engineering from the University of Florence, Florence, Italy, in 2006 and he is currently working towards his PhD degree at Ecole Polytechnique Fédérale de Lausanne (EPFL). His research interests include analysis, design and realization of implantable, small and UWB antennas.

Jean-F. ZURCHER was born in Vevey, Switzerland, in 1951. He graduated with the degree of Electrical Engineer from Ecole Polytechnique Fédérale de Lausanne (Lausanne Institute of Technology) in 1974. He is presently employed as permanent scientific associate with the Laboratoire d'Electromagnétisme et d'Acoustique EPFL, where he is the manager of the microwave laboratory. His main interest lies in the domain of microstrip circuits and antennas. In 1988, he invented the SSFIP concept ("Strip Slot Foam Inverted Patch antenna"), which became a commercial product. He is presently developing instrumentation and techniques for the measurement of near fields of planar structures and microwave materials measurement and imaging. Mr. Zürcher is the author or co-author of about 125 publications, chapters in books and papers presented at international conferences. He is one of the two authors of the book "Broadband Patch Antennas", published by Artech in 1995. He holds 8 patents.

Juan R. MOSIG was born in Cadiz, Spain. He received the Electrical Engineer degree from the Universidad Politecnica de Madrid, Madrid, Spain, in 1973, and the Ph.D. degree from the Ecole Polytechnique Fédérale de Lausanne (EPFL), Lausanne, Switzerland, in 1983. Since 1991, he has been a professor at EPFL and since 2000, he has been the head of the Laboratory of Electromagnetics and Acoustics (LEMA) at EPFL. In 1984, he was a visiting research associate with the Rochester Institute of Technology, Rochester, NY, and Syracuse University, Syracuse, NY. He has also held scientific appointments with the University of Rennes, France, the University of Nice, France, the Technical University of Denmark at Lyngby and the University of Colorado at Boulder, USA. At EPFL, he is currently a co-Director of the College of Humanities and the Chairman of the EPFL Space Center, conducting many Swiss research projects for the European Space Agency (ESA). He is a also a Fellow of the IEEE, the chairperson of the European COST Action on Antennas "ASSIST" (2007–2011) and a founding member and acting chair of the European Association&Conferences on Antennas and Propagation (EurAAP and EuCAP). Dr. Mosig has authored five chapters in books on planar antennas and circuits and over 100 peer-reviewed journal papers. His current research interests include electromagnetic theory, numerical methods, and planar antennas.

Anja K. SKRIVERVIK got her electrical engineering degree from Ecole Polytechnique Fédérale de Lausanne in 1986, and her PhD from the same institution in 1992. After a passage at the University of Rennes and the Industry, she returned to EPFL as an assistant professor in 1996, and is now a "Professeur titulaire" at this institution. Her teaching activities include courses on microwaves and on antennas. Her research activities include electrically small antennas, multi-frequency and ultra wideband antennas, numerical techniques for electromagnetic and microwave and millimeter wave MEMS. She is an author or co-author of more than 100 scientific publications. She is very active in European collaboration and European projects. She is currently the chairperson of the Swiss URSI, the Swiss representative for COST action 297 and a member of the board of the Center for High Speed Wireless Communications of the Swedish Foundation for Strategic Research.